Height-Gradient-Based Method for Occlusion Detection in True Orthophoto Generation

Henrique Cândido de Oliveira, Mauricio Galo, and Aluir Porfírio Dal Poz

***Abstract*—High-quality orthophotos are essential elements in cartographic databases that are required for engineering projects. Urban areas usually have many tall buildings, causing occlusions in aerial images. These occlusions can be severe depending on the height of the buildings, geometry of the imaging system, and image acquisition viewpoint. A product where no occlusion areas appear is called true orthophoto, and occlusion detection is a key step in its generation. This process requires a set of aerial images and surface representation, together with metadata and acquisition system information. This letter addresses a new approach for occlusion detection. The central idea that allows the development of the proposed method is based on the analysis of the surface height gradient at certain sampled directions, guiding the identification of occluded regions in the aerial images. A novel metric is introduced based on the height gradient computed along an available digital surface model, which can be obtained by different techniques. The refinement of the occlusion area is made by applying one morphological operator, aiming to fill some gaps in the detected occlusion areas. In order to validate the proposed approach, simulated and real data were used. The quality assessment was based on both visual and numerical analyses. For this methodology, the numerical analysis showed high completeness and correctness values, indicating that the proposed approach works properly.**

***Index Terms*—Height gradient, light detection and ranging (LiDAR), occlusion detection, true orthophoto.**

I. Introduction

Nowadays, geospatial data have a fundamental importance in a wide range of engineering projects, and remotely sensed images have been used almost exclusively for geospatial data generation. Several urban applications need these images, such as urban planning and change detections.

The orthophoto is free from errors caused by relief displacement and platform attitude. In order to transform an aerial or orbital image into a conventional orthophoto, it is necessary to have the camera model, along with its interior orientation parameter (IOP) and exterior orientation parameter (EOP), and a digital terrain model (DTM), which represents only the terrain surface.

Manuscript received May 5, 2015; accepted July 14, 2015. Date of publication August 17, 2015; date of current version October 27, 2015. The work of H. C. de Oliveira was supported by the Fundação de Amparo à Pesquisa do Estado de São Paulo (FAPESP) under Grant 2013/21647-2.

H. C. de Oliveira is with the Graduation Program in Cartographic Science, São Paulo State University, Presidente Prudente, SP 19060-900, Brazil (e-mail: henrique.cartografia@gmail.com).

M. Galo and A. P. Dal Poz are with the Department of Cartography, São Paulo State University, Presidente Prudente, SP 19060-900, Brazil (e-mail: galo@fct.unesp.br; aluir@fct.unesp.br).

Color versions of one or more of the figures in this paper are available online at http://ieeexplore.ieee.org.

Digital Object Identifier 10.1109/LGRS.2015.2459671

Orthophotos portraying urban areas with many tall buildings tend to show them projected onto the terrain. As a result, many targets, such as streets, parks, and low buildings, are partially or totally occluded by these tall buildings. These unrepresented portions in conventional orthophotos are the so-called occlusion areas. The occlusion detection is very important since these areas prevent complete interpretation and extraction of spatial information.

In order to mitigate the drawback discussed earlier, related to the use of conventional orthophotos in urban applications, it is necessary to replace the DTM by a digital surface model (DSM) in its creation. The DSM represents the terrain and also all the objects above the ground, such as buildings, trees, and bridges. The DSM may be obtained by light detection and ranging (LiDAR) technology [1] and also by others techniques such as the dense image matching [2]. The use of a DSM allows the generation of a special category of orthophoto—the true orthophoto. In this product, all targets are represented in true orthographic positions, no matter if they are on the ground or aboveground.

As mentioned, the key step for true orthophoto generation is the occlusion detection. If an occlusion area is identified, the gray levels of its pixels are obtained by looking for a corresponding area not occluded in available adjacent images. Thus, a visibility analysis is accomplished to find the occluded areas in all adjacent images. The true orthophoto is completely generated after filling all occlusion areas with the proper radiometric information [3]–[5].

Although the orthophoto generation process is well known, it is still being studied by the scientific community, as can be seen in recent works [5]–[11]. Most research efforts have been concentrated in the main bottleneck of the true orthophoto generation process: occlusion detection. Another point that highlights the importance of these research studies is that few digital photogrammetric workstations (DPWs) have a module dedicated to automatic generation of true orthophotos, as can be seen in [12]. This is an indication that research is still necessary to increase the use of photogrammetric applications with efficient tools for true orthophoto generation. Some of these DPWs use a digital building model (DBM), where 3-D models represent all features in an urban scene. The main disadvantage of using a DBM in true orthophoto generation is the high cost and time consumption necessary to produce this type of model.

Existing methods for this purpose are based either on the Z-buffer method and its variations [5]–[8] or on the angle-based method [7]–[10]. The Z-buffer method compares distances between the perspective center (PC) and the DSM cells that

1545-598X © 2015 IEEE. Personal use is permitted, but republication/redistribution requires IEEE permission.
See http://www.ieee.org/publications_standards/publications/rights/index.html for more information.

are competing for the same image pixel—the closest DSM cell is labeled as visible. The angle-based method analyzes sequentially the off-nadir angles to the straight line formed by the PC and the DSM cells in a radial direction starting from the nadir point—a sudden decrease of the angles indicates an occluded cell. A common drawback of both methods is the need of analyzing all cells in a gridded DSM. Particularly, the Z-buffer method presents the false visibility problem when applied to scenes with tall and narrow buildings, which is not a problem for the angle-based method [7], [10].

In view of the motivation discussed earlier, this letter proposes a novel method for occlusion detection in aerial images. It is based on the analysis of DSM height gradients along a specific direction followed by the postprocessing by using mathematical morphology. This letter extends the work of [11] and is organized as follows: Section II presents the proposed method for occlusion detection; Section III presents and discusses some results and comparisons; and Section IV finalizes this letter with the presentation of the main conclusion and future work.

II. Height-Gradient-Based Method

As aforementioned, the key point in true orthophoto generation is to locate the occlusion areas, which can be accomplished by different techniques. In this letter, we propose the use of the height-gradient metric. In order to introduce the basic idea of this metric, let us consider DSM profiles taken in radial directions from the nadir point. The height gradients between adjacent cells are computed for each profile. The gradient attribute has the following useful property: the initial point of each occlusion segment has a negative height gradient. This means that the height gradients along radial directions are useful for determining initial points of occlusion sections. After determining an initial occlusion point by the criterion of negative height gradient, a simple geometric operation is necessary for determining the end of occlusion for each radial direction. This procedure enables determination of the extension of an occlusion in a specific radial direction. The whole occlusion area is then determined by analyzing successive adjacent radial directions. Details on the proposed method are presented in the next sections.

Profile Determination: For each groundel (ground element or DSM cell) on the DSM border (underlying DSM portion corresponding to the image) connected to the nadir point, i.e., PC′ (see Fig. 1), it is possible to determine one radial direction using Bresenham's algorithm [13]. Since the point PC′ is unique for one specific image, the radial profiles can be obtained by connecting the fixed PC′ to each groundel on the image border, assuming that the DSM covers the entire image.

Gradient Computation: The coordinates (X, Y, Z) of each groundel on a DSM profile are known in the DSM coordinate system. However, as a DSM profile is two dimensional, the position of each groundel can be defined using only two coordinates, i.e., distance r between the point PC′ and the selected groundel and the height Z of the same groundel. In order to compute the height gradient between every two consecutive groundels in one profile, it is assumed that the selected profile

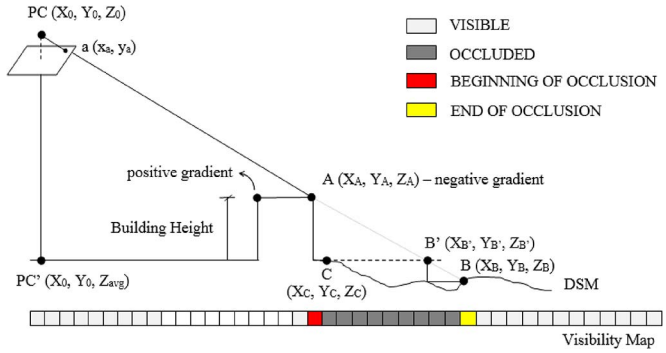

Fig. 1. Hypothetical scene and necessary elements to apply the proposed method (profile in a radial direction).

is composed of n groundels having each one a Z_i value (i.e., the altitude), with $i = \{1, 2, \ldots, n-1, n\}$. From these definitions, the height gradient $(\partial Z/\partial r)$ at each groundel along the selected profile is approximate by finite differences, as follows:

$$\begin{aligned} \text{If } 1 \leq i < n, \quad & \frac{\partial Z}{\partial r_i} \cong \frac{Z_{i+1} - Z_i}{r_{i+1} - r_i} \\ \text{If } i = n, \quad & \frac{\partial Z}{\partial r_i} \cong \frac{Z_n - Z_{n-1}}{r_n - r_{n-1}} \end{aligned} \tag{1}$$

where r_i is the position of the ith groundel along the selected profile.

In this way, every groundel can be labeled with a positive or negative sign, in accordance with the sign of the derivatives, i.e., if $\partial Z/\partial r > 0$ or $\partial Z/\partial r < 0$, respectively. The positive gradients correspond to the profile segments having growing altitudes. Furthermore, these positive gradients are visible from the PC. On the other hand, negative gradients correspond to the profile segments having decreasing altitudes. However, the negative gradient is a helpful attribute for localizing the first groundel of an occluded profile segment from the PC viewpoint (see Fig. 1). This property enables us to formulate the following rule: First occurring groundels with negative gradients are the initial points of occluded profile segments. As shown in the next section, the initial groundels of occluded profile segments are the key point for determining the endpoint of every occluded profile segment.

It is important to mention that some factors, such as artifacts resulted from the interpolation process for generating the DSM, low density and accuracy of points obtained by an acquisition process (for example, LiDAR), etc., may generate an undesirable effect that prejudices the initial occlusion groundel identification by the height-gradient method. All these effects may cause false height gradient signs and, consequently, false occlusion identification, which may generate unexpected results, such as false visibility. As a result, detected occluded areas usually require some postprocessing steps for refining them, which will be the subject of the last topic of this section.

Determination of Occlusion Endpoints: In order to know the entire occluded profile segments, it is necessary to determine their endpoints. Fig. 1 presents the principle of the proposed method for determining the endpoint of an occluded profile segment. The initial point (A) of the occlusion is located on the

boundary of the building, where the height gradient is negative. It can be seen that from the PC viewpoint, the endpoint of this occlusion is located at point B. As shown in Fig. 1, point B can be defined as the intersection between the straight line, containing point A and its image point (a), with the DSM.

The necessary elements for the endpoint computation (B) of any occlusion segment are as follows: the coordinates (X_A, Y_A, Z_A) of point A in the object space, the EOP, the IOP, and the groundel coordinates of the radial profile.

To calculate the correspondent image point of A, it is necessary to do an intermediate mathematical transformation. The image coordinates (x_a, y_a) of point A are computed based on the collinearity equation [18], as follows:

$$x_a = -f \cdot \left[\frac{m_{11}\cdot(X_A - X_0) + m_{12}\cdot(Y_A - Y_0) + m_{13}\cdot(Z_A - Z_0)}{m_{31}\cdot(X_A - X_0) + m_{32}\cdot(Y_A - Y_0) + m_{33}\cdot(Z_A - Z_0)}\right]$$
$$y_a = -f \cdot \left[\frac{m_{21}\cdot(X_A - X_0) + m_{22}\cdot(Y_A - Y_0) + m_{23}\cdot(Z_A - Z_0)}{m_{31}\cdot(X_A - X_0) + m_{32}\cdot(Y_A - Y_0) + m_{33}\cdot(Z_A - Z_0)}\right] \quad (2)$$

where f is the focal length of the camera; m_{ij} are the elements of the rotation matrix M, which are computed as a function of attitude angles of the camera at the image exposure time; and X_0, Y_0, and Z_0 are the coordinates of PC at the image exposure time.

The EOPs (attitude angles and PC coordinates) can be estimated by the aerial triangulation process or space resection, or it can also be obtained by a direct georeferencing using the Global Navigation Satellite System and Inertial Measurement Unit systems embedded in the imagery acquisition system.

The final step involves projecting the image point (x_a, y_a) obtained by (2) onto the DSM, thus obtaining the endpoint B of the occluded profile segment. This can be efficiently accomplished by the Makorovic monoplotting method [15]. This method is based on the inverse collinearity equation [14], i.e.,

$$X_B = X_0 + (Z_B - Z_0) \cdot \left[\frac{m_{11}\cdot x_a + m_{21}\cdot y_a - m_{31}\cdot f}{m_{13}\cdot x_a + m_{23}\cdot y_a - m_{33}\cdot f}\right]$$
$$Y_B = Y_0 + (Z_B - Z_0) \cdot \left[\frac{m_{12}\cdot x_a + m_{22}\cdot y_a - m_{32}\cdot f}{m_{13}\cdot x_a + m_{23}\cdot y_a - m_{33}\cdot f}\right]. \quad (3)$$

In this equation, all variables are known, except the height Z_B.

Makorovic's algorithm [15] solves this problem iteratively, starting with the height of point C on the ground (see Fig. 1). Using the definition of the height gradient given by (1), the height of point C can be estimated by the following equation: $Z_C = Z_A + (\partial Z/\partial r_A)(r_c - r_A)$. Makorovic's algorithm proceeds as follows: 1) Assign Z_C to Z_B and use (3) to compute the coordinates $(X_{B'}, Y_{B'})$ of point B'; 2) interpolate $Z_{B'}$ from the DSM using $(X_{B'}, Y_{B'})$; and 3) assign $Z_{B'}$ to Z_B and repeat steps 1 and 2 until no significant coordinate changes in the Z component is verified. After convergence, the stabilized coordinates are X_B, Y_B, and Z_B, i.e., the coordinates of the endpoint B of the occluded profile segment.

As shown in Fig. 1, points A and B correspond to the initial groundel (in red) and the end groundel (in yellow), respectively. These two groundels, along with the interior groundels (in dark gray), define an occluded radial segment. Groundels labeled as visible and invisible form a 1-D structure known as the visibility map for a radial direction. This structure, which is extended to all radial profiles, results in a 2-D visibility map, or simply visibility map for the entire image.

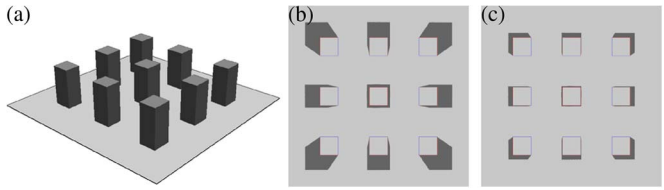

Fig. 2. (a) Simulated DSM. Occlusion results obtained by varying the PC altitudes. (b) Lower. (c) Higher.

Refinement of Occlusion by Mathematical Morphology: This proposed occlusion detection method results in a radial line pattern effect [see Fig. 4(b)]. There are two main reasons for the appearance of this effect.

First, as the radial profiles converge at the nadir point (PC′), superposition between adjacent radial profiles occurs near this point, and gaps between adjacent radial profiles become progressively larger in the direction of the DSM border. This means that gaps' effect is not critical near the PC′, but it increases when moving away from it. A possible solution for the gap problem is the densification of radial profiles, but it can increase the computational effort.

Second, as described in Section II, some radial directions may not have initial occlusion groundels correctly associated with corresponding radial direction, resulting in false visibility. This leads to radial gaps in the visibility map.

Both types of radial gaps can be efficiently filled *a posteriori* by applying appropriate mathematical morphological operators [16], without any significant increase of computational effort. Basically, we propose the use of a simple morphologic dilation operator with a structuring element in a cross format (dimension: 3 × 3) to fill the occlusion gaps detected along adjacent radial profiles. It is relevant to highlight that this morphological operation is applied only to occluded segments of the binary visibility map.

III. Experiments and Discussion

The experimental analysis of the proposed method was based on simulated and real data. In the following, we present and discuss the obtained results and some comparisons with angle-based and Z-buffer methods.

Experiments With Simulated Data: The validation of the proposed method using simulated data was based on a DSM representing a 3-D scenario [see Fig. 2(a)]. It is composed by a simple 3 × 3 tall-building configuration on a flat surface. The generated gridded DSM contains about one million points, with a resolution of 1 m. This configuration is similar to the one presented in [7], thus allowing a relative comparison between both results.

Figs. 2 and 3 present the data and the results obtained by the proposed height-gradient-based method.

By comparing the results shown in Figs. 2 and 3 with those obtained by the angle-based method in [7], it is possible to

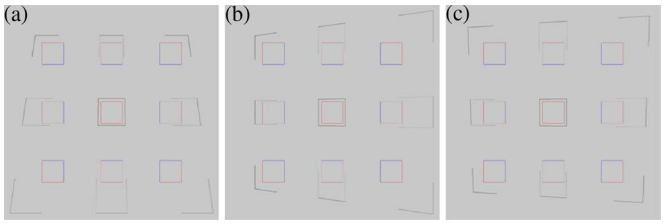

Fig. 3. Occlusion limits obtained by varying the PC attitude. (a) Using $\omega = 2^\circ$ and $\varphi = \kappa = 0^\circ$. (b) Using $\varphi = 2^\circ$ and $\omega = \kappa = 0^\circ$. (c) Using $\omega = 2^\circ$, $\varphi = 2^\circ$ and $\kappa = 110^\circ$.

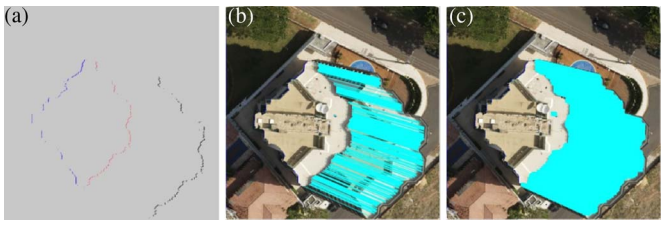

Fig. 4. Main steps of the proposed method in Experiment 1.

realize that both results show the same pattern, varying only in their extensions, which may be different due to the use of different flying heights or different building heights, or both.

Experiment 1 With Real Data: The first experiment using real data was made with a pair of digital aerial images at an average scale of 1:10 000 and with a ground sample distance (GSD) of about 0.07 m and a 0.07-m resolution DSM in a rugged terrain area, which was generated by using a LiDAR point cloud with an average density of 8 points/m^2. The DSM was created using a triangulated irregular network structure to interpolate the grid altitudes.

The result of occlusion detection obtained for the experiments is presented step by step in Fig. 4:

(a) gradient map: positive gradient (blue), negative (red), and end of occlusion (black) obtained by the proposed method;
(b) occlusion lines connecting the beginning of the occlusion and its estimated end (obtained in step a);
(c) occluded area refined by the morphological dilation operator.

Experiment 2 With Real Data: The second experiment was carried out by using an aerial image (GSD $\approx$ 0.11 m) at an average scale of 1/1000 and a DSM with a resolution of about 0.11 m. The data set is the same used by [7]. This allows a relative assessment between the results obtained by the angle-based, Z-buffer, and height-gradient-based methods (see Fig. 5).

Quality Analysis of the Proposed Method: In general, the results obtained by using simulated and real data showed that the proposed method works properly. Results presented in Figs. 2 and 3 allow a visual analysis regarding the coherence and also a comparison with the angular-based method, which was presented in [7]. On the other hand, the results using a real data set show correct occlusion detection and also clear improvement by using the morphological dilation operator in the refinement process.

As shown in Fig. 4(c), the morphological dilation operator successfully repaired the gaps between segments of occluded

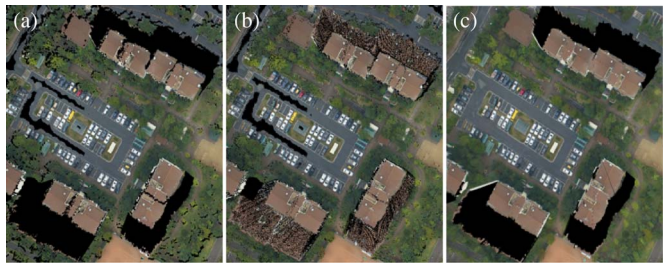

Fig. 5. Occlusion detection method—Time consuming. (a) Angle-based method—30 s. (b) Z-buffer method—1 min 24 s. (c) Height-gradient-based method—21 s.

TABLE I
COMPLETENESS AND CORRECTNESS FOR THE DETECTED OCCLUSION

Exp.	Occlusion	Completeness (%)	Correctness (%)
1	Without Morphology	63.29	99.89
	With Morphology	90.44	95.27

radial profiles. It is possible to note that the occluded area does not have its radiometric pixel values, which must be obtained from corresponding non-occluded areas in adjacent images.

Afterward, the quality assessment of the obtained results was computed based on the following indicators: the completeness and the correctness. Both indicators are computed from the occlusion areas automatically, which were extracted by the proposed algorithm, and a corresponding reference polygon was manually extracted by an operator. Completeness measures the percentage of a reference polygon detected as an occlusion area by the method being evaluated. Correctness measures the percentage of elements detected as occlusion by the method, which is in fact inside the reference polygon. Additional details can be found in [17] and [18].

Based on these indicators, a quantitative assessment of the result was carried out for the initial occlusion [see Fig. 4(b)] and final occlusion areas [see Fig. 4(c)]. The reference polygon was created manually for the occlusion area in this assessment. Table I shows the quantitative assessment values for the first experiment.

It is possible to verify that the use of the morphological dilation operator increases the completeness value significantly. This improvement is useful for true orthophoto generation, because the more complete the detected occlusion areas, the better the true orthophoto will be. On the other hand, the correctness decreases with the use of a mathematical morphological operator. However, this reduction does not affect the results, because even if a portion is labeled as occluded, it will be refilled in the true orthophoto using radiometric information from adjacent images.

Fig. 5 shows a comparison among the methodology proposed in [7]—the angle-based method [see Fig. 5(a)], the Z-buffer method [see Fig. 5(b)], and the new approach presented in this work [see Fig. 5(c)]. It is possible to verify the coherence in the results, as well as compatibility between angle and height-gradient-based methods, mainly for the tall buildings, which are responsible for most occlusion areas. The proposed method utilizes a threshold to identify the negative gradients. This is the reason why the trees or low buildings, which do not have so much impact on the true orthophoto, are not detected as the

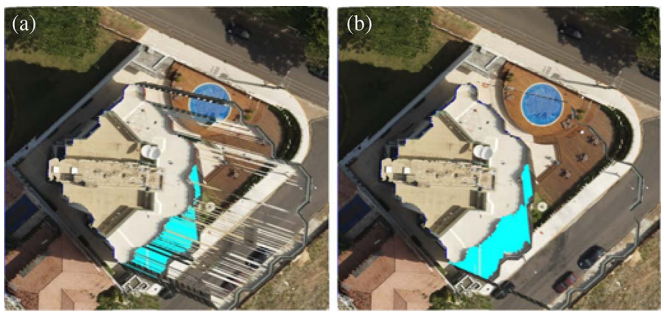

Fig. 6. Generated true orthophotos. (a) Using the initial occlusion area. (b) Using the occlusion area refined by the morphological approach.

beginning of occlusion. The proposed method also shows the capability to overcome the drawback presented in the Z-buffer method.

Assuming all occlusion areas were delimited, the corresponding digital number of each pixel can be transferred from adjacent images, aiming the generation of the true orthophoto. This search for the correspondent image pixels in the adjacent image was done for Experiment 1. Fig. 6(a) presents the true orthophoto generated by using the initial occlusion area [see Fig. 4(b)]. Fig. 6(b) shows the true orthophoto using the final occlusion areas obtained after applying the morphological refining approach [see Fig. 4(c)]. It is important to highlight that some pixels of the true orthophoto keep appearing in cyan color (occlusion areas). This happens because these pixels are not visible in any image from the set of images used in these experiments.

Fig. 6 shows that the postprocessing of the occlusion areas by using the morphological dilation operator was very useful and efficient. The improvement of the results by applying the morphological dilation process is clear.

IV. Conclusion and Future Work

Occlusion detection is a key point in true orthophoto generation. Some methods for this detection can be found in the literature, and each method has its own characteristics. An alternative metric for occlusion detection is proposed in this letter. This metric is based on the height gradient that can be used to obtain the beginning of the occlusion area in radial directions. To minimize the occurrence of spurious gradients due to noises in the DSM data and DSM densification, and to fill the occlusion areas, a morphological postprocessing step was introduced.

Experiments using synthetic data showed that the results obtained with the proposed method and the angle-based method are coherent and similar. For the experiments on real data in which aerial images and the DSM obtained by LiDAR techniques were used, the average completeness and correctness were around 90%. Based on these experiments, and by the comparison with the angle-based and Z-buffer methods, it is possible to observe the coherence of the results and the potential of the proposed method for occlusion detection. In addition, the method seems to be faster than the angle-based and Z-buffer methods. In fact, the results obtained for the second experiment (see Fig. 5) showed that the processing time of the height-gradient-based method was 1.4 and 4 times faster than the angle-based and Z-buffer methods, respectively.

Future work includes some efforts for improving the proposed method, e.g., reduction of the noise level in the height gradient, parameter settings for more general classes of buildings, and treatment of multiple occlusions.

Acknowledgment

The authors would like to thank Dr. A. F. Habib (Purdue University) and Dr. C. Kim (Myongi University) for the supply of the data set and the code to generate results for comparison, as well as the Department of Cartography, São Paulo State University (UNESP), Presidente Prudente, Brazil, for the infrastructure and supply of the data used in this work.

References

[1] A. Wehr and U. Lohr, "Airborne laser scanning—An introduction and overview," *ISPRS J. Photogramm. Remote Sens.*, vol. 54, no. 2/3, pp. 68–82, Jul. 1999.

[2] N. Haala, M. Cramer, and K. Jacobsen, "The German camera evaluation project—Results from the geometry group," in *Proc. Int. Arch. Photogramm., Remote Sens. Spatial Inf. Sci.*, Calgary, AB, Canada, 2010, vol. 38, pp. 1–6.

[3] A. Criminisi, P. Perez, and K. Toyama, "Region filling and object removal by exemplar based image in painting," *IEEE Trans. Image Process.*, vol. 13, no. 9, pp. 1200–1212, Sep. 2004.

[4] F. Amhar, J. Jansa, and C. Ries, "The generation of true orthophotos using a 3D building model in conjunction with a conventional DTM," *Int. Arch. Photogramm. Remote Sens.*, vol. 32, pp. 16–22, 1998.

[5] C. Kim, " Object-based integration of photogrammetry and LiDAR data for accurate reconstruction and visualization of building models," Ph.D. dissertation, Dept. Geomatics Eng., Univ. Calgary, Calgary, AB, Canada, 2008.

[6] J. Y. Rau, N. Y. Chen, and L. C. Chen, "True orthophoto generation of built-up areas using multi-view images," *Photogramm. Eng. Remote Sens.*, vol. 68, no. 6, pp. 581–588, Jun. 2002.

[7] A. F. Habib, E. Kim, and C. Kim, "New methodologies for true orthophoto generation," *Photogramm. Eng. Remote Sens.*, vol. 73, no. 1, pp. 25–36, Jan. 2007.

[8] K. I. Bang, A. F. Habib, S. W. Shin, and K. O. Kim, "Comparative analysis of alternative methodologies for true ortho-photo generation from high resolution satellite imagery," in *Proc. ASPRS Annu. Conf.*, Tampa, FL, USA, 2007, pp. 1–12.

[9] R. Antequera *et al.*, "Development of an integrated system of true orthorectification. The Altais LRTO system," *Int. Arch. Photogramm., Remote Sens. Spatial Inf. Sci.*, vol. 37, Part B4, pp. 253–258, 2008.

[10] C. Zhong, H. Li, and X. Huang, "A fast and effective approach to generate true orthophoto in built-up area," *Sensor Rev.*, vol. 31, no. 4, pp. 341–348, 2011.

[11] H. C. Oliveira and M. Galo, "Occlusion detection by height gradient for true orthophoto generation, using LiDAR data," *Int. Arch. Photogramm., Remote Sens. Spatial Inf. Sci.*, vol. XL-1/W, pp. 275–280, 2013.

[12] Gim International, Lemmens, The Netherlands, Product Survey: Digital Photogrammetric Workstations. 2011, (21 Mar. 2013). [Online]. Available: http://www.gim-international.com/productsurvey/id48-Digital_Photogrammetric_Workstations,_December.html

[13] D. F. Rogers, *Procedural Elements for Computer Graphics*. New York, NY, USA: McGraw-Hill, 1985, pp. 34–42.

[14] E. M. Mikhail, J. S. Bethel, and J. C. McGlone, *Introduction to Modern Photogrammetry*. New York, NY, USA: Wiley, 2001.

[15] M. Radwan and B. Makarovic, "Digital mono-plotting system-improvements and tests," *ITC J.*, vol. 3, pp. 511–533, 1980.

[16] R. C. Gonzalez and R. E. Woods, *Digital Image Processing*. 3rd ed. Upper Saddle River, NJ, USA: Prentice-Hall, 2007.

[17] A. J. Fazan and A. P. Dal Poz, "Rectilinear building roof contour extraction based on snakes and dynamic programming," *Int. J. Appl. Earth Observ. Geoinf.*, vol. 25, pp. 1–10, Dec. 2013.

[18] C. Wiedemann, C. Heipke, H. Mayer, and O. Jamet, "Empirical evaluation of automatically extracted road axes," in *Empirical Evaluation Methods in Computer Vision*. Washington, DC, USA: IEEE Comput. Soc. Press, 1998, pp. 172–187.